Two-Dimensional Axisymmetric Finite Element Simulation of Lower Hybrid Wave with an Iterative Scheme

Fumiya ADACHI, Naoto TSUJII, Akira EJIRI, Kouji SHINOHARA, Seowon JANG, Yi PENG, Kotaro IWASAKI, Yu-Ting LIN, Zhengnan JIANG, Yiming TIAN, Yangguang JIANG, Shengyu WANG, Yijin XIONG and Masaru YOSHIDA

University of Tokyo, Kashiwa 277-0882, Japan

(Received 27 October 2023 / Accepted 25 June 2024)

Simulating waves in hot plasmas in configuration space is a difficult problem because of the non-local property of the plasma response, which makes the wave equation an integro-differential one. In this research, we conducted an axisymmetric hot plasma full wave simulation at the lower hybrid frequency range with the finite element method. Kinetic effects were introduced in the direction parallel to the magnetic field. We implemented the code so that it can handle an arbitrary velocity distribution function to introduce electron kinetics. An iterative method was utilized to introduce the non-local hot plasma contribution, which is more memory efficient than direct solving. The hot plasma perturbed current density was iteratively calculated in our scheme. For the present simulation, we used the plasma equilibrium obtained by the experiment with the TST-2 spherical tokamak, which is located at the University of Tokyo. The simulation with the realistic profiles successfully converged. The electron heating power deposition profile was estimated for the obtained electric field solutions.

© *2024 The Japan Society of Plasma Science and Nuclear Fusion Research*

Keywords: lower hybrid wave, full wave simulation, finite element method

DOI: 10.1585/pfr.19.1403026

1. Introduction

Accurate analyses of waves in plasmas need a wave theory that takes into account the kinetic response of the plasma, namely, the hot plasma model. The difficult point of the hot plasma full wave simulations is that the plasma response becomes non-local, expressed as an integral operator. This makes the wave equation to be solved an integro-differential equation in configuration space. Because of this characteristic, many of the previous full wave calculations were based on the spectral representation [1, 2]. The plasma response becomes an algebraic product in wavenumber space, making the implementation straightforward. This natural choice of simulation domain, however, requires the inversion of a large and dense matrix, and the problem becomes computationally expensive. Also, owing to the use of a global Fourier basis, it is inefficient to model complex geometries such as the scrape off layer and the antenna structure. In real experiments, interactions of waves with plasmas in the scrape off layer and/or with launchers could lead to deteriorated efficiency of heating and current drive. The interactions need to be simulated accurately. Full wave simulations in configuration space with the finite element method (FEM) can efficiently handle complicated structures with flexible meshing, such as using finer meshing where more meshing is needed. The FEM enables integrated modelling of the core plasma and edge regions.

Lower hybrid (LH) current drive has been conducted in many tokamak experiments [3, 4]. Traditionally, ray tracing has been used to analyze waves in the LH frequency range. The technique solves the geometrical optics equations assuming the Wenzel-Kramers-Brillouin (WKB) approximation. It succeeded, for example, in explaining experimentally obtained current drive efficiency [5]. However, coupling of LH waves from the antenna to the plasma cannot be treated within the framework because the LH wave has a low-density cutoff at $\omega = \omega_{\mathrm{pe}}$, where $\omega/2\pi$ is the frequency of the LH wave and $\omega_{\mathrm{pe}}/2\pi$ is the electron plasma frequency. Ray tracing must start somewhere inside the plasma where the LH waves are not evanescent. In addition, when the LH waves approach the cutoff layer, the wavelength and the plasma scale length become comparable and the WKB approximation may break down. This could be a problem in the multi-pass damping regime. Full wave simulations can overcome these difficulties.

Previous FEM full wave simulations solved the integro-differential wave equation with an iterative scheme [6–8]. An iterative scheme consumes more time than a direct solver, but can work with less computational resources. In Ref. [6], two-dimensional finite element full wave simulations of the LH waves were implemented. A possible problem is that their scheme included division by the electric field to calculate an effective dielectric. It may be inaccurate at interferences where the electric field becomes almost zero. In this work, we present a different

author's e-mail: adachi@fusion.k.u-tokyo.ac.jp

© 2024 The Japan Society of Plasma Science and Nuclear Fusion Research

iterative scheme to simulate a two-dimensional LH wave model. In our scheme, the hot plasma perturbed current density that is consistent with the global wave simulation is iteratively calculated.

The organization of this paper is as follows. Section 2 briefly describes the wave physics and the implementation of our code. Section 3 shows the results from the homogeneous hot plasma simulation of LH waves and verifies the present scheme. In Sec. 4, we simulate LH waves in a hot plasma with a realistic plasma equilibrium and show the results. Finally, in Sec. 5, we summarize our work.

2. Implementation of LH Wave Model

Assuming a time dependence $\propto \mathrm{e}^{\mathrm{i}\omega t}$, high frequency waves are described by

$$\nabla \times (\nabla \times \mathbf{E}) - \frac{\omega^2}{c^2}\mathbf{E} = -\mathrm{i}\omega\mu_0\mathbf{j}, \tag{1}$$

where $\mathbf{E}$ is the electric field, $\mathbf{j}$ is the current density, c is the speed of light in vacuum and μ_0 is the vacuum permeability. In wave analysis, we usually assume a linear plasma response to waves:

$$\mathbf{j}(\mathbf{r}) = \hat{\boldsymbol{\sigma}} \cdot \mathbf{E}. \tag{2}$$

Here, $\hat{\boldsymbol{\sigma}}$ is the plasma conductivity. With Eq. (2), Eq. (1) becomes the Helmholtz equation:

$$\nabla \times (\nabla \times \mathbf{E}) - \frac{\omega^2}{c^2}\hat{\mathbf{K}} \cdot \mathbf{E} = \mathbf{0}, \tag{3}$$

where

$$\hat{\mathbf{K}} = \mathbf{1} - \frac{\mathrm{i}\hat{\boldsymbol{\sigma}}}{\epsilon_0\omega}, \tag{4}$$

$\hat{\mathbf{K}}$ is the plasma dielectric and ϵ_0 is the vacuum permittivity. The plasma dielectric or the plasma conductivity determines wave propagation and damping. In general, the plasma dielectric and the plasma conductivity are integral operators. Therefore, the wave equations Eqs. (1) and (3) become integro-differential equations. However, when we consider a uniform plasma or assume local homogeneity, the plasma dielectric and the plasma conductivity become algebraic multiplication in the spectral domain.

The major linear damping mechanism for the LH waves is electron Landau damping. The corresponding term of the conductivity can be obtained as below by following the derivation of [9]. Here, we consider one-dimensional Vlasov equation of species s:

$$\frac{\partial f_s}{\partial t} + v_z\frac{\partial f_s}{\partial z} + \frac{q_s E}{m_s}\frac{\partial f_s}{\partial v_z} = 0, \tag{5}$$

where $f_s(z, v_z, t)$ is a velocity distribution function, q_s is a charge, m_s is a mass. Considering a perturbation f_{1s} around the equilibrium distribution f_{0s}, Eq. (5) can be linearized to

$$\frac{\mathrm{d}f_{s1}}{\mathrm{d}t} = \left(\frac{\partial}{\partial t} + v_z\frac{\partial}{\partial z}\right)f_{s1} = -\frac{q_s E}{m_s}\frac{\partial f_{s0}}{\partial v_z}. \tag{6}$$

Equation (6) can be solved by integrating along the unperturbed particle orbit:

$$f_{s1}(z, v_z, t) = -\frac{q_s}{m_s}\int_{-\infty}^{t}\mathrm{d}t' E(z', t')\frac{\partial f_{s0}}{\partial v_z}(z', v_z), \tag{7}$$

where $z - z' = v_z(t - t')$. By taking the velocity moment, the perturbed current density becomes

$$j_{s1}(z) = \int_{-\infty}^{\infty}\mathrm{d}z'\left(-\frac{{q_s}^2}{m_s}\int_0^{\infty}\mathrm{d}\tau\frac{z - z'}{\tau^2}\frac{\partial f_{s0}}{\partial v_z}\mathrm{e}^{\mathrm{i}\omega\tau}\right)E(z'). \tag{8}$$

To obtain a simplified expression of the conductivity operator in configuration space, we have changed the variables of integration: $(t', v_z) \to (t', z')$ and set $\tau = t - t'$.

When we assume local homogeneity $f_{s0}(z', v_z) \approx f_{s0}(z, v_z)$, the conductivity kernel is

$$\sigma_{\mathrm{hot},s}(z - z') = -\frac{{q_s}^2}{m_s}\int_0^{\infty}\mathrm{d}\tau\frac{z - z'}{\tau^2}\frac{\partial f_{s0}}{\partial v_z}\mathrm{e}^{\mathrm{i}\omega\tau}. \tag{9}$$

The real part of Eq. (9) corresponds to electron Landau damping, and the imaginary part introduces a kinetic correction in wave propagation. Note that in Eq. (8), the current density j_{s1} is obtained as a convolution of the conductivity kernel and the electric field. With $\omega/2\pi = 200\,\mathrm{MHz}$, an electron density of $3\times10^{17}\,\mathrm{m}^{-3}$, and a velocity distribution function shown in Fig. 1, the conductivity kernel becomes as shown in Fig. 2. The velocity distribution function has two characteristic temperatures: the bulk temperature $T_\mathrm{b} = 15\,\mathrm{eV}$ and the tail temperature $T_\mathrm{t} = 20\,\mathrm{keV}$. For $v_z < 1.5v_{\mathrm{th,b}}$, the distribution follows a Maxwellian distribution with temperature T_b, and for $v_z > 1.5v_{\mathrm{th,b}}$, the distribution follows a Maxwellian distribution with temperature T_t. Here, $v_{\mathrm{th,b}}$ is the thermal velocity of bulk electrons, defined as $v_{\mathrm{th,b}} = \sqrt{2T_\mathrm{b}/m_\mathrm{e}}$.

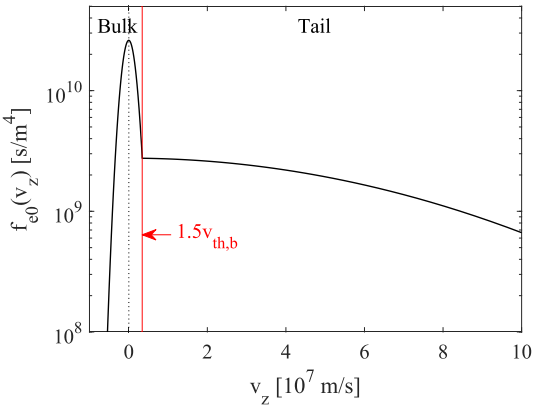

Fig. 1 Example of the electron velocity distribution function with the electron density of $3 \times 10^{17}\,\mathrm{m}^{-3}$. It switches from the Maxwellian with the bulk temperature of 15 eV to the Maxwellian with the tail temperature of 20 keV. The switching velocity is 1.5 times the bulk thermal velocity in this case.

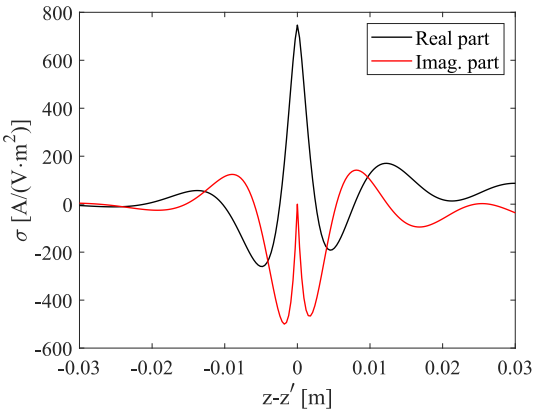

Fig. 2 Example of the conductivity kernel expressed in Eq. (9). The wave frequency of $\omega/2\pi = 200\,\mathrm{MHz}$, and the electron velocity distribution function as shown in Fig. 1 are assumed.

Our simulation used the plasma dielectric which introduced electron Landau damping:

$$\hat{\mathbf{K}} = \mathbf{K}_{\mathrm{cold},\perp} + \hat{\mathbf{K}}_{\mathrm{hot},\parallel} = \begin{pmatrix} S & \mathrm{i}D & 0 \\ -\mathrm{i}D & S & 0 \\ 0 & 0 & 0 \end{pmatrix} + \hat{z}\hat{z}(P + \hat{\chi}_{\mathrm{ELD}}), \tag{10}$$

where S, D and P are the Stix parameters as defined in [10], and

$$\hat{\chi}_{\mathrm{ELD}} = -\frac{\mathrm{i}\hat{\sigma}_{\mathrm{ELD}}}{\epsilon_0\omega}, \tag{11}$$

$$\hat{\sigma}_{\mathrm{ELD}} = \Re\hat{\sigma}_{\mathrm{hot,e}}. \tag{12}$$

Equation (10) is written in the magnetic coordinate system where the magnetic field is in the $\hat{z}$ direction. In the cylindrical coordinates (R, ϕ, Z), the plasma dielectric $\mathbf{K}_c$ can be obtained by rotating the coordinates as

$$\mathbf{K}_c = \mathbf{U}^{-1} \cdot \mathbf{K} \cdot \mathbf{U}, \tag{13}$$

where

$$\mathbf{U} = \begin{pmatrix} \sqrt{1-b_R{}^2} & \dfrac{-b_R b_\phi}{\sqrt{1-b_R{}^2}} & \dfrac{-b_R b_Z}{\sqrt{1-b_R{}^2}} \\ 0 & \dfrac{b_Z}{\sqrt{1-b_R{}^2}} & \dfrac{-b_\phi}{\sqrt{1-b_R{}^2}} \\ b_R & b_\phi & b_Z \end{pmatrix}, \tag{14}$$

b_R, b_ϕ, b_Z are the three components of the normalized magnetic field in the cylindrical coordinates:

$$\frac{\mathbf{B}}{|\mathbf{B}|} = b_R\hat{R} + b_\phi\hat{\phi} + b_Z\hat{Z}, \tag{15}$$

and $\mathbf{B}$ is the magnetic field.

Here we introduce two expressions for the perturbed current density:

$$\mathbf{j}_{\mathrm{NL}} = \hat{z}\int \mathrm{d}z'\sigma_{\mathrm{ELD}}(z-z')E_z(z'), \tag{16}$$

$$\mathbf{j}_{\mathrm{A}} = \hat{z}\sigma_{\mathrm{ELD}}(k_{\parallel 0})E_z, \tag{17}$$

where $k_{\parallel 0}$ is a prescribed parallel wavenumber and $\sigma_{\mathrm{hot,e}}(k_\parallel)$ is the Fourier transform of $\sigma_{\mathrm{hot,e}}(z)$. $\mathbf{j}_{\mathrm{NL}}$ is the fully non-local expression of the current density and $\mathbf{j}_{\mathrm{A}}$ is the approximate expression of the current density with the prescribed wave number. Also, we define $\delta\mathbf{j}$ as the difference between those two quantities:

$$\delta\mathbf{j} = \mathbf{j}_{\mathrm{NL}} - \mathbf{j}_{\mathrm{A}}. \tag{18}$$

Since Eqs. (1) and (3) are integro-differential equations, we solved the wave equation iteratively as follows:

$$\begin{cases} \nabla\times\left(\nabla\times\mathbf{E}^{(N)}\right) - \dfrac{\omega^2}{c^2}(\mathbf{K}_{\mathrm{cold},\perp} + \mathbf{K}_{\mathrm{hot},\parallel}(k_{\parallel 0}))\cdot\mathbf{E}^{(N)} \\ \qquad = -\mathrm{i}\omega\mu_0\mathbf{I}^{(N-1)} \\ \mathbf{I}^{(N-1)} = \mathcal{A}\left(\delta\mathbf{j}^{(N-1)}, \delta\mathbf{j}^{(N-2)}, \ldots, \delta\mathbf{j}^{(0)}\right), \end{cases} \tag{19}$$

where N is the iteration index, $\mathbf{K}_{\mathrm{hot},\parallel}(k_\parallel)$ is the Fourier transform of the kernel $\mathbf{K}_{\mathrm{hot},\parallel}(z)$, and $\mathcal{A}$ symbolizes the operation of Anderson acceleration [11]. In order to improve convergence, the non-local plasma effect was split into the current density and the plasma dielectric. Only the difference between the non-local expression and the approximate expression was iterated. In addition, we utilized Anderson acceleration, one of the vector extrapolation methods. In our simulation, we used all the previously obtained solutions for Anderson acceleration to prepare the next input $\mathbf{I}$ at every iteration. The RF module of COMSOL Multiphysics [12] was used to solve the wave equation in Eq. (19) with the FEM. By driving the RF module and evaluating the perturbed current density with MATLAB [13], we iteratively calculated wave propagation and damping.

3. Homogeneous Plasma Simulations and Results

First, we simulated LH waves in a homogeneous plasma described in Fig. 3 to verify the iterative scheme explained in Sec. 2. The electron density was $1 \times 10^{17}\,\mathrm{m}^{-3}$, and the electron velocity distribution function was Maxwellian with a temperature of 500 eV. The magnetic field with a magnitude of 0.04 T was tilted for 92° from the $\hat{x}$ direction. This is to simulate the tilted magnetic field in a tokamak because of the poloidal field. The length of the simulation domain in the $\hat{y}$ direction was the same as the wavelength of the LH waves in the $\hat{y}$ direction, and the parallel wavenumber was scanned by changing the wavenumber in the $\hat{y}$ direction k_y at the boundary. We added an artificial damping region to avoid the reflection of the wave at the edge.

The waves were excited with the electric field boundary condition; the $\hat{y}$ component of the electric field was imposed as $E_y = E_{\mathrm{ant}}\sin(k_y y)$, where $E_{\mathrm{ant}} = 1\,\mathrm{V/m}$. The wave frequency was 200 MHz. The imposed wavenumber in the $\hat{y}$ direction k_y was used as a prescribed parallel wavenumber $k_{\parallel 0}$. In this tilted magnetic field geome-

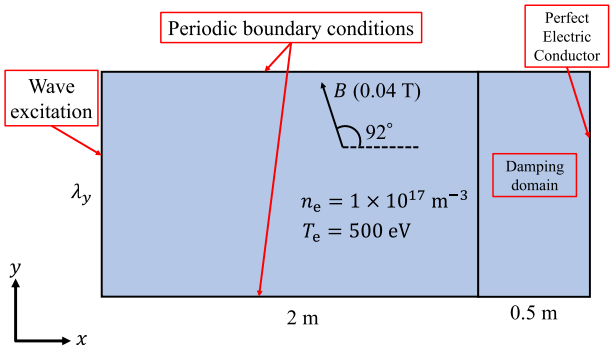

Fig. 3 Settings for the homogeneous plasma simulation.

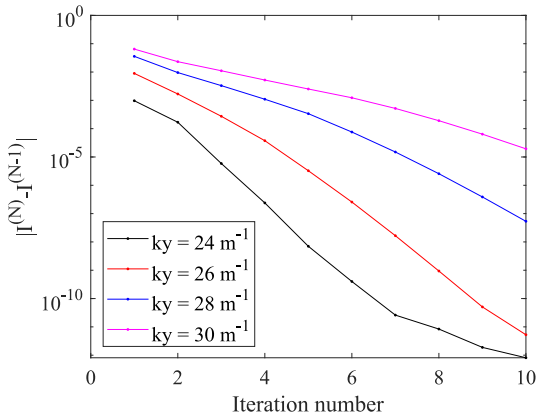

Fig. 4 Residual error for the homogeneous plasma simulation.

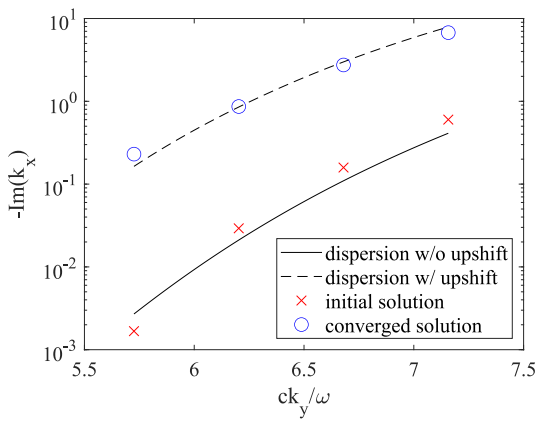

Fig. 5 Imaginary part of the wavenumber in the $\hat{x}$ direction. The values for the initial and converged solutions and the analytical values are shown.

try, the parallel wavenumber of the analytical solution is larger than k_y, and the wavenumber correction was iteratively added to the solution.

Figure 4 shows the residual error for the homogeneous plasma simulation. The residual error for all the simulations became sufficiently small successfully. Figure 5 shows the imaginary part of the wavenumber in the $\hat{x}$ direction. As expected, since the wavenumber upshift occurred, the wave damping became stronger for the converged solution than the initial solution. Also, as k_y increased in the chosen parameter range, the wave damping became stronger. This agreed with the characteristic of Landau damping. The converged solutions were almost the same as the dispersion relation with wavenumber upshift. The dispersion relation with the upshift was obtained by solving the dispersion relation with

$$k_{\parallel} = k_x \frac{B_x}{B} + k_y \frac{B_y}{B}. \tag{20}$$

The relation without the upshift was obtained in the same way, but by neglecting the first term on the right-hand side of Eq. (20).

We can roughly evaluate wave damping in a hot plasma by approximating a wavenumber in the direction parallel to the magnetic field with a toroidal wavenumber (k_y in this model) [14]. The parallel wavenumber, however, deviates from the toroidal wavenumber because of the poloidal magnetic field. It is necessary to introduce this difference into a model for quantitatively accurate simulations. With the present iterative scheme, wave damping can be calculated with more accuracy by using the integral form of the hot plasma perturbed current density.

4. Axisymmetric Full Wave Simulation and Results

TST-2 is a spherical tokamak located at the University of Tokyo. Its major radius is 0.36 m, its minor radius is 0.23 m, and its toroidal field strength is < 0.3 T. Three capacitively coupled combline antennas are installed at the outer-midplane, at the top, and at the outer-off-midplane [15–17]. The parallel refractive index is 5.5 for the outer-midplane launch antenna, 4.9 for the top launch antenna, and 13 for the outer-off-midplane launch antenna, respectively. A source of 100 kW is available for each antenna operating at a frequency of 200 MHz. Typically, the discharge duration is about 80 ms. The electron density and the electron temperature profiles are measured with Thomson scattering diagnostics, and the fitted curves at the flat top of a discharge were used in the present simulation.

We conducted a two-dimensional axisymmetric full wave simulation on a poloidal plane. Toroidal mode number, which is a conserved quantity in an axisymmetric system, was $n_\phi = 20$ and the wave frequency was $\omega/2\pi = 200$ MHz. The bulk electron temperature and the electron density were assumed to be flux functions. The magnetic flux surfaces were obtained by EFIT [18] reconstruction and is shown in Fig. 6. The bulk electron temperature and the electron density profiles used in the simulation are shown in Fig. 7. These are the equilibrium profiles obtained in the experiment with the TST-2 spherical tokamak. We used the solutions from a Fokker-Planck solver CQL3D [19] coupled with ray tracing code GENRAY [20] for the electron velocity distribution function. Figure 8 shows the used electron velocity distribution func-

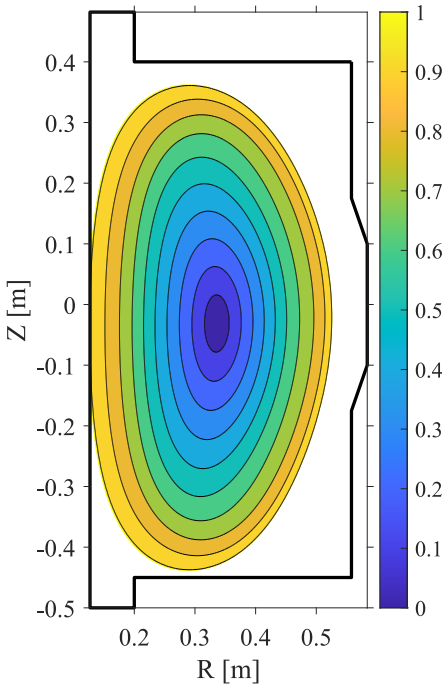

Fig. 6 Normalized toroidal flux obtained by EFIT. The simulated area is encircled by the black solid lines.

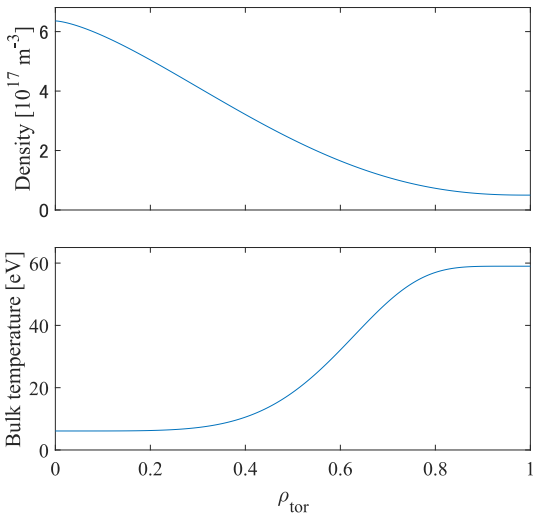

Fig. 7 Bulk electron density and electron temperature profiles of the LH start-up plasma in TST-2.

tion. This is obtained by integrating the GENRAY-CQL3D simulation result over the perpendicular velocity. Outside the last closed flux surface (the white region in Fig. 6), the bulk electron temperature and the electron density were assumed to be constant and the same as that on the last closed flux surface. The waves were excited with the electric field boundary condition; the toroidal component of the electric field was imposed as follows on the outer edge around the midplane.

$$E_\phi = 1\,\mathrm{V/m} \quad (-0.5L < z < 0.5L), \tag{21}$$

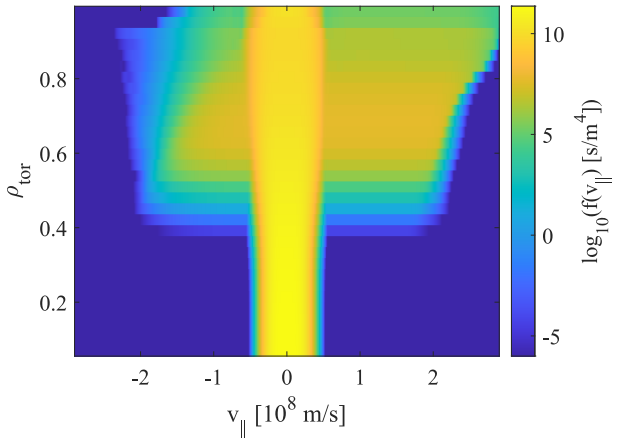

Fig. 8 Electron velocity distribution function used in the axisymmetric simulation. This is obtained from the GENRAY-CQL3D simulation result.

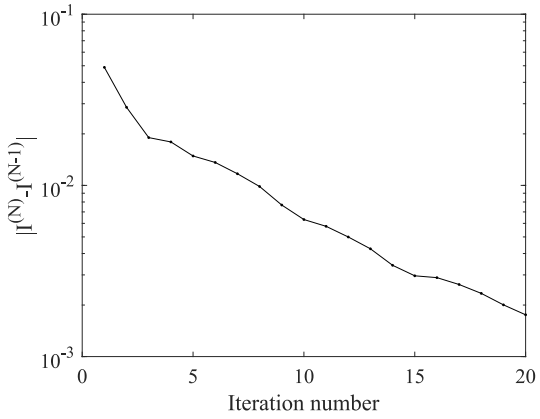

Fig. 9 Residual error for the axisymmetric simulation.

with $L = 0.15\,\mathrm{m}$. The other walls were assumed to be perfect electric conductors. We initialized the iteration with $\mathbf{I}^{(-1)} = \mathbf{0}$, that is, by considering only the approximate analytic damping. To calculate the approximate current density, Eq. (17), we prescribed toroidal wavenumber $k_{\mathrm{tor}} = n_\phi/R$ as an approximation for the parallel wavenumber. The current density component corresponding to the difference between $\sigma_{\mathrm{hot,e}}(k_\parallel)$ and $\sigma_{\mathrm{hot,e}}(k_{\mathrm{tor}})$ was iteratively added to the model.

Figure 9 shows the residual error for the axisymmetric simulation. The relative change in the total power deposition is shown in Fig. 10. Here $P^{(N)}$ is the electron heating power density $\Re(\mathbf{j}_{\mathrm{NL}} \cdot \mathbf{E}^*)/2$ integrated over the simulation domain at the Nth iteration. Although the error of the total power deposition was fluctuating, it still stayed at the order of 10^{-4} after about 15 iterations. The converged solution is shown in Fig. 11. Figure 12 shows the profile of the heating power density averaged over the toroidal flux surfaces at the initial iteration and the 20th iteration, and the result from a ray tracing code which only considers electron Landau damping. In the simulated plasma, the parallel

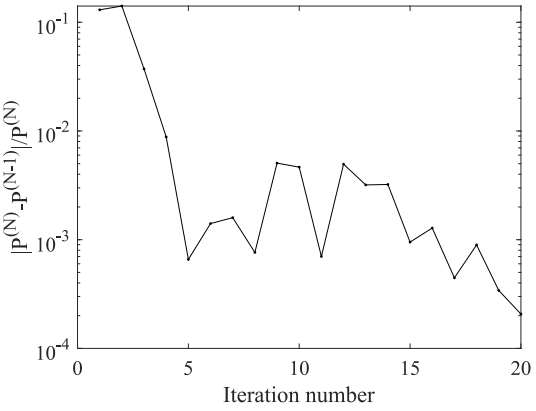

Fig. 10 Relative change of the deposited power. The change was less than 10^{-3} after 17 iterations.

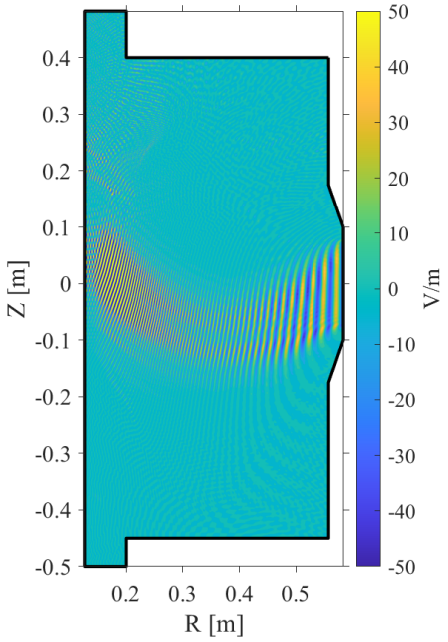

Fig. 11 Converged electric field solution. The parallel component is shown.

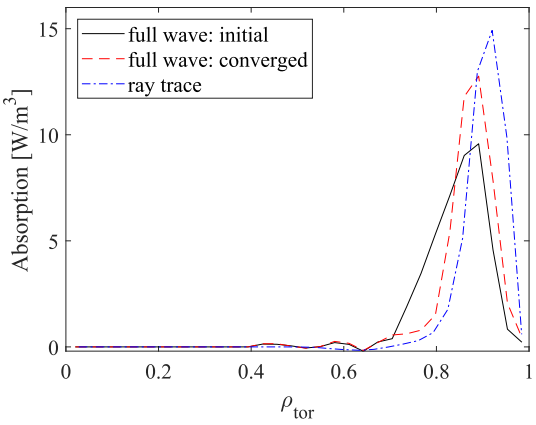

Fig. 12 Flux surface averaged electron heating power density profile.

wavenumber of the waves experienced a downshift due to the poloidal magnetic field [21]. The actual wave absorption must be weaker than the approximate analytic absorption (= initial absorption). Therefore, as the iteration went on, the region where the wave was damped moved outward. Note that the waves were launched from the low field side and damped near the inner walls with a single pass in the present simulation. The converged solution from the full wave simulation showed absorption near the plasma edge, and the characteristic matched that of the ray tracing result. However, they showed a slightly different location of absorption. Full wave effects such as diffraction are not included in ray tracing. Also, it is non-trivial how to set the initial wavenumber for each ray in ray tracing, which affects the location of absorption. The discrepancy may come from these reasons.

5. Summary

We have developed a new LH full wave simulation code with the FEM scheme, utilizing the commercial FEM solver. The new code is able to handle an arbitrary electron velocity distribution function. The non-local hot plasma contribution was implemented with an iterative scheme. The electron Landau damping was introduced as a non-local hot plasma response. In order to improve convergence, we split the hot plasma effect into the plasma dielectric and the current density, and made use of Anderson acceleration. With the newly developed code, firstly we have conducted a homogeneous plasma simulation and verified the code. Secondly, we have conducted an axisymmetric simulation of the LH waves with the realistic electron bulk density and temperature profiles. The simulation successfully converged. The electron heating power profile was estimated for the converged electric field and the result agreed well with that of the ray tracing code.

Interactions of waves with plasmas in the scrape off layer and/or with launchers could be problematic for heating and current drive. It is necessary to consider the interactions in real experiments and future reactors. The previous codes using spectral representation cannot efficiently describe physics in such complex geometries. The FEM enables integrated modelling of the antenna structure and the hot core plasma, but the integral formulation of plasma response must be employed. We introduced the integral form perturbed current density in the present FEM model. In the future extensions, the integrated modelling with our FEM model will be tested. Also, the present model neglects the kinetic propagation correction and handles only the real part of the conductivity kernel. The full treatment of the kinetic expressions remains as a future work.

[1] M. Brambilla and T. Krücken, Nucl. Fusion **28**, 1813 (1988).
[2] E.F. Jaeger, L.A. Berry, E. D'Azvedo, D.B. Batchelor *et al.*, Phys. Plasmas **8**, 1573 (2001).

[3] S. Shiraiwa, S. Ide, S. Itoh, O. Mitarai *et al.*, Phys. Rev. Lett. **92**, 035001 (2004).
[4] V.V. Dyachenko, O.N. Shcherbinin, E.Z. Gusakov, V.K. Gusev *et al.*, Nucl. Fusion **55**, 113001 (2015).
[5] P.T. Bonoli, J. Ko, R. Parker, A.E. Schmidt *et al.*, Phys. Plasmas **15**, 0561117 (2008).
[6] O. Meneghini, S. Shiraiwa and R. Parker, Phys. Plasmas **16**, 090701 (2009).
[7] D. Green and L. Berry, Comput. Phys. Commun. **185**, 736 (2014).
[8] P. Vallejos, T. Hellsten and T. Johnson, J. Phys. Conf. Ser. **1125**, 012020 (2018).
[9] J.E. Drummond, R.A. Gerwin and B.G. Springer, J. Nucl. Energy, Part C Plasma Phys. **2**, 98 (1961).
[10] T. Stix, *Waves in Plasmas* (American Institute of Physics, New York, 1992).
[11] H. Walker and P. Ni, SIAM J. Numer. Anal. **49**, 1715 (2011).
[12] COMSOL Multiphysics, www.comsol.com, COMSOL AB, Stockholm, Sweden.
[13] MATLAB, www.mathworks.com, The MathWorks Inc., Natick, MA, USA.
[14] C. Lau, L.A. Berry, E.F. Jaeger and N. Bertelli, Plasma Phys. Control. Fusion **61**, 045008 (2019).
[15] T. Shinya, Y. Takase, S. Yajima, C. Moeller *et al.*, Nucl. Fusion **57**, 036006 (2017).
[16] S. Yajima, Y. Takase, Y. Tajiri, Y. Takei *et al.*, Nucl. Fusion **59**, 066004 (2019).
[17] Y. Ko, N. Tsujii, A. Ejiri, O. Watanabe *et al.*, Nucl. Fusion **63**, 126015 (2023).
[18] L.L. Lao, H. St. John, R.D. Stambaugh, A.G. Kellman *et al.*, Nucl. Fusion **25**, 1611 (1985).
[19] R.W. Harvey and M.G. McCoy, Proc. IAEA TCM on Advances in Sim. and Modelling of Thermonuclear Plasmas, 489 (1992).
[20] A.P. Smirnov, R.W. Harvey and K. Kupfer, Bull. Am. Phys. Soc. **39**, 1626 (1994).
[21] P.T. Bonoli and E. Ott, Phys. Fluids **25**, 359 (1982).